Applied Catalysis B: Environmental 211 (2017) 323–336

Contents lists available at ScienceDirect

Applied Catalysis B: Environmental

journal homepage: www.elsevier.com/locate/apcatb

Research paper

A multi-technique approach to disclose the reaction mechanism of dimethyl carbonate synthesis over amino-modified SBA-15 catalysts

Valentina Crocellà [a,*,1], Tommaso Tabanelli [b,1], Jenny G. Vitillo [a], Daniele Costenaro [c], Chiara Bisio [c,d], Fabrizio Cavani [b,*], Silvia Bordiga [a]

[a] Dipartimento di Chimica, NIS, INSTM Reference Centre, Università di Torino, Via Quarello 15/A, 10135 Torino, Italy
[b] Dipartimento di Chimica Industriale Toso Montanari, Università di Bologna, Viale Risorgimento 4, 40136 Bologna, Italy
[c] Dipartimento di Scienze e Innovazione Tecnologica (DISIT) and Interdisciplinary Nano-SiSTeMI Centre, Università del Piemonte Orientale, Via T. Michel 11, 15121 Alessandria, Italy
[d] ISTM-CNR Istituto di Scienze e Tecnologie Molecolari, via G. Venezian 21, Milano, Italy

ARTICLE INFO

Article history:
Received 9 January 2017
Received in revised form 31 March 2017
Accepted 5 April 2017
Available online 6 April 2017

Keywords:
Amine-modified SBA-15
Transesterification reaction
Dimethyl carbonate
In situ FT-IR spectroscopy
Methanol activation
Intermediate stabilization

ABSTRACT

A series of amine-modified SBA-15 was employed as catalysts in the carbonate interchange reaction of ethylene carbonate (EC) with methanol to produce dimethyl carbonate (DMC). These materials exhibited good catalytic performances that strongly depended on the reaction temperature. A multi-technique approach was employed to disclose the role played by the different amine chains in driving the whole reaction. To this purpose, *in situ* FT-IR experiments were combined with theoretical calculations in order to explain the catalytic results observed in the presence of catalysts with different basic strength. A close correlation was found between the number and the nature of the alkylamine chains present in the SBA-15 pores and the capacity of the catalyst to activate the reagent molecules, as well as to stabilize the reaction intermediate. It was demonstrated that the ability of the catalyst to dissociatively adsorb methanol is the key factor for the proper choice of the catalytic system. Moreover, the capacity of the catalyst to stabilize the reaction intermediate has to be considered to allow the reaction to proceed so obtaining the desired final product (DMC).

1. Introduction

Organic carbonates are becoming industrially viable alternatives to toxic reactants (*e.g.*, phosgene), through what has been termed the "green carbonyl route". Amongst them, the interest towards dimethyl carbonate (DMC) has grown rapidly during latest years, thanks to its clean and non-polluting nature and to its versatile reactivity [1–3]. Current DMC production is higher than 0.5 Mt y^{-1}, but its potential in several fields could further boost its production. For example, DMC is an environmentally benign building block to produce intermediates for different organic processes: it can be used as a methylation and carbonylation agent to replace highly toxic and corrosive reagents such as methyl halides, phosgene and dimethyl sulfate [4,5]. DMC is also used as an ideal fuel additive due to its high oxygen content, as precursor for the production of polycarbonate resins, and as electrolyte for lithium batteries [6,7].

Currently, the industrial processes to produce DMC (*i.e.* phosgenation and oxidative carbonylation of methanol or carbonylation of methylnitrile) involve high risk or expensive compounds such as phosgene, nitric oxide and carbon monoxide [8,9]. For these reasons, the development of environmentally compatible processes for the production of DMC has gained considerable attention. In particular, three are the greener routes to obtain this molecule: (i) the direct reaction between carbon dioxide and methanol, though this process has important thermodynamic limitations [10,11]; (ii) the methanolysis of urea [12]; and (iii) the transesterification of ethylene carbonate (EC) with methanol [13–16]. In particular, this last reaction has been recognized as a promising process due to its environmentally benign nature and high yield of DMC.

Moreover, the employment of EC as reagent enables phosgene-free operations and the utilization of carbon dioxide as feedstock, cyclic carbonates being produced by the insertion of CO_2 into the corresponding epoxides. The two-step reaction for the production of DMC starting from ethylene oxide (EO) and CO_2 is reported in Scheme 1.

* Corresponding authors.
E-mail addresses: valentina.crocella@unito.it (V. Crocellà), fabrizio.cavani@unibo.it (F. Cavani).
[1] These authors contributed equally to this work.

http://dx.doi.org/10.1016/j.apcatb.2017.04.013
0926-3373/

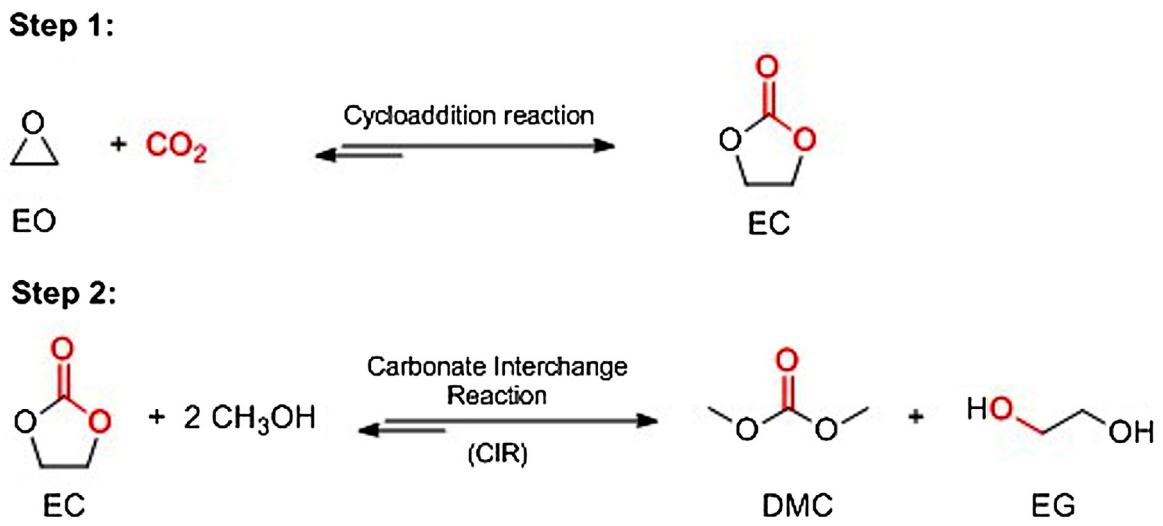

Scheme 1. Two-step reaction for the synthesis of DMC.

In the first step, the epoxide reacts with CO_2 producing EC while in the second step, after the cyclic carbonate separation and purification, the EC undergoes transesterification with methanol to DMC and to the corresponding glycol. Nowadays, this two-step process constitutes a greener and sustainable alternative for the production of DMC with respect to the more common procedures adopted industrially. However, this process presents a not-negligible drawback: the two steps of the process are carried out in two separate reactors.

The CO_2 coupling with epoxides (step 1) is a highly exothermic reaction ($\Delta H_R = -140$ kJ/mol), and both Lewis acid and basic catalysts can be used, being able to initiate the reaction by activating either the CO_2 or the epoxide (or both at the same time). A wide number of catalytic systems have been reported to be active for this reaction, of both homogeneous (metal complexes of Al, Cr, Co, Zn and Sn, metal halides, ammonium salts and ionic liquids) [10,17–27] and heterogeneous nature (supported halides salts on oxides or zeolites, metal oxides like MgO, Al-Mg mixed oxides and ZnO-SiO_2, Cs-modified zeolites and amine-functionalized silica catalysts) [13,28–31]. On the other hand, both acid and basic catalysts are reported to be also active in the EC transesterification step [29,32–34].

Theoretically, the use of a catalytic system able to promote both steps would open the possibility to investigate the one-pot synthesis of DMC in a single reactor, so reducing the energy consumption, the starting investment and the overall production costs. Different heterogeneous (for example, basic metal oxides and base supported molecular sieves) and homogeneous catalysts have been studied for the one-pot synthesis of DMC from carbon dioxide, epoxides and methanol [29,33,35–38]. It is clear that a good catalyst for the one-pot synthesis of DMC has to be active in both the reaction steps with good conversions and yields, and to minimize the parasite reactions (like the methanolysis of the epoxide).

Amino-functionalized mesoporous silicas have been extensively studied as catalysts in different base-catalyzed reactions, as for example transesterification of esters, Knoevenagel and Claisen-Schmidt condensations and Henry addition [39–43]. Zhang et al. [31] reported very good catalytic results for a series of amine-functionalized silica catalysts in the chemical fixation of carbon dioxide to cyclic carbonates, *i.e.* in the first of the two steps of the above reported reaction (see Scheme 1). Thanks to their basic nature, amino-modified silicas could be good candidates to be employed as catalysts also in the second step of the one-pot DMC synthesis. For this reason, in the present work, the reactivity of different amino-functionalized mesoporous silicas has been also investigated in the transesterification reaction of EC with methanol to obtain DMC. In this reaction, the EC undergoes two consecutive carbonate interchange reactions (CIRs) with methanol, as reported in Scheme 2, in order to yield, firstly, the intermediate 2-hydroxyethylmethyl carbonate (from hereafter referred to as HEMC), and, finally, the desired DMC with ethylene glycol (EG) as co-product.

In this work, a multi-technique approach has been employed to disclose the reaction mechanism, *i.e.* to understand the role played by different amine chains in: (i) activating the reagent molecules, (ii) stabilizing the reaction intermediate and (iii) driving the whole reaction. To this purpose, *in situ* FT-IR experimental data were combined with theoretical calculations in order to explain the catalytic results observed in the presence of catalysts with different basic strength.

2. Experimental

2.1. Synthesis of amine-modified SBA-15 silicas

Hexagonally ordered mesoporous silica of the SBA-15 family was functionalized using various organic silanes, containing a different number of amino groups (see Scheme 3), in order to tune the basic features (*i.e.* basic sites strength and density) of the final material.

Two different approaches were employed for the insertion of the organic moiety in the mesoporous silica structure: (i) a post-synthesis surface grafting and (ii) a one-pot synthesis.

2.1.1. Post synthesis grafting

In this synthetic pathway, the starting SBA-15 was synthesized as described by Zhao et al. [44]. Briefly, the commercial block copolymer Pluronic P123 (8 g), used as the template, was dissolved in 60 mL of deionized water at 35 °C for 24 h. The obtained solution was acidified with 240 mL of HCl 2 M and then tetraethyl orthosilicate (TEOS, 17 g) was added. After 24 h stirring, the gel was introduced in a Teflon autoclave (125 mL capacity, Anton PARR 4748) and heated at 100 °C for 24 h. At the end of this procedure, the samples were filtered, washed with deionized water and dried for 36 h at 120 °C. Finally, the material was calcined at 550 °C for 5 h in an air flow (100 mL/min) in order to remove the organic template and obtain the SBA-15 structure.

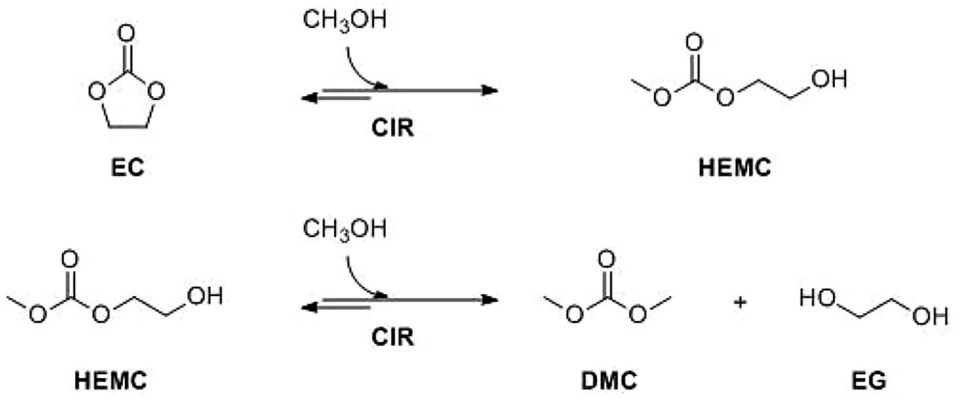

Scheme 2. Carbonate interchange reaction of EC with methanol to obtain DMC and EG.

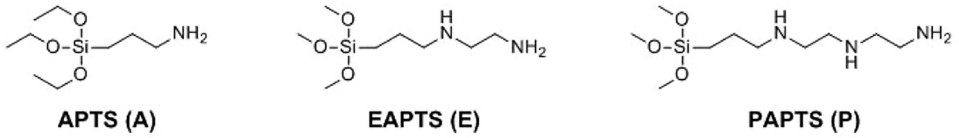

Scheme 3. Organic silanes used for the synthesis of functionalized SBA-15: 3-aminopropyltriethoxysilane (APTS), *N*-[3-(trimethoxysilyl)propyl]-ethylenediamine (EAPTS) and *N*-[3-(trimethoxysilyl)propyl]-diethylenetriamine (PAPTS).

Afterwards, the bare SBA-15 was activated under vacuum at 150 °C for 3 h in order to clean the surface from physisorbed water and then stirred for 20 h at 50 °C in a solution of the desired organic silane (50% w/w in toluene). Sample was then filtered and washed with toluene and diethylether in order to remove the unreacted silane and finally dried at 50 °C obtaining the desired RNH_2-SBA-15 material. Three different samples (hereafter referred to as A-SBA-15, E-SBA-15, P-SBA-15) were obtained starting from the organic silanes reported in Scheme 3.

2.1.2. One-pot synthesis

In this second synthetic pathway the organic silane (in this case only EAPTS) was added to the solution containing the silica precursor before the hydrothermal treatment. In particular, after the addition of TEOS the sol was stirred for two hours and then a 10 mol% of the desired organosilane was added to the gel and stirred for 24 h. The so obtained gel underwent a hydrothermal treatment (24 h at 100 °C), then it was filtered, washed with deionized water and dried at 120 °C for 16 h. Finally, the excess of organic template was removed by extraction with ethanol. After this step, the functionalized silicas were dried again at 120 °C for 16 h. The recovered sample was named E-SBA-15(OP).

2.2. Catalysts characterization

X-ray powder diffraction (XRD) patterns were collected with a Thermo ARL 'XTRA-048 diffractometer with a CuKα (λ = 1.54 Å) radiation. The diffractograms were recorded in the 2θ range of 0.7–3° at the rate of 1°/min with a step size of 0.02°.

N_2 adsorption-desorption isotherms were collected at 77 K by means of a Quantachrome Autosorb iQ2 analyzer in the 10^{-7}-1 relative pressure range. Before the analysis all samples were activated in vacuum at 150 °C for 3 h (residual pressure $p < 10^{-6}$ Torr) in the degas port of the adsorption analyzer. Specific surface areas were determined by using the Brunauer–Emmett–Teller (BET) model, in the 0.01–0.1 relative pressure range. Pore size distributions were obtained by applying the Non Localized Density Functional Theory (NL-DFT) method (N_2 silica kernel based on a cylindrical pore model).

C-H-N elemental contents were determined using an EA 3000 elemental analyser (EuroVector). Helium and oxygen at 120 and 35 kPa pressure were used, respectively. For each material, the measurement were repeated three times.

FT-IR spectra were collected at 4 cm^{-1} resolution on a Thermo Electron Corporation FT Nicolet 5700 Spectrometer. The samples were examined in the form of self-supporting pellets mechanically protected with a pure gold frame. Self-supporting pellets were placed into a homemade IR cell with KBr windows permanently attached to vacuum line (residual pressure: 10^{-4} mbar), allowing all treatments and adsorption-desorption experiments to be carried out *in situ*.

Thermogravimetric analysis (TGA) were performed on a Setaram SETSYS Evolution instrument under O_2 (gas flow rate 100 mL/min), heating the samples from 30 °C to 800 °C with a rate of 5 °C/min.

2.3. Catalytic tests

Preliminary tests for DMC synthesis were performed with a molar ratio of methanol to EC equal to 10, in a simple two-necked flask equipped with two reflux condensers, at the reflux temperature of methanol (reaction temperature 65 °C), and at atmospheric pressure.

The high-pressure reaction tests were performed in a 50 mL stainless steel autoclave. In a standard reaction procedure, the reagents and the catalyst were charged inside the autoclave, then the system was sealed and purged with N_2, the reactor was pressurized at the desired starting pressure and heating was started. The time zero of the reaction was taken when the reactor reaches the desired reaction temperature.

Before each reactivity test, the catalysts were "activated" one night in static oven at 120 °C to remove the physisorbed water, and charged into the reactor at 5% w/w compared to the limiting reagent (EC).

After the reactivity tests, the autoclave was cooled with an ice bath down to room temperature, pressure was released and 100 μL of the mixture was diluted in 10 mL acetone (HPLC grade, Sigma-Aldrich); 10 μL of decane was added to the solution and used as

internal standard. The final solution was filtered in order to remove the heterogeneous catalyst and finally analyzed by means of GC.

The compounds of interest were analysed and quantified using a Thermo Focus GC gas-chromatograph equipped with a non-polar capillary column Agilent HP-5 (5% phenyl–95% methylsiloxane) as reported in details in Section S2 of the Supplementary material.

2.4. In situ *FT-IR measurements*

FT-IR spectra were collected at 2 cm^{-1} resolution on a Bruker Vertex 70 spectrophotometer, equipped with a MCT cryodetector, at "beam temperature" (BT), *i.e.* the temperature reached by samples under the IR beam (around 50 °C). The samples were examined in the form of self-supporting pellets mechanically protected with a pure gold frame. Before each measurement, all samples were activated in controlled atmosphere, at 150 °C for 2 h, using a home-made quartz IR cell, equipped with KBr windows and characterized by a very small optical path (2 mm). The cell was connected to a conventional high-vacuum glass line, equipped with mechanical and turbo molecular pumps (capable of a residual pressure $p < 10^{-4}$ mbar), that allows *in situ* adsorption/desorption measurements of molecular probes and reactivity experiments.

2.5. *Computational methods*

The calculations have been performed with the *Gaussian 09* software package [45]. The amines grafted on the SBA-15 surfaces have been modeled by considering the corresponding organic silane molecule, where each methoxy group was substituted by a −OH capping atom. Both the neutral (APTS, EAPTS, PAPTS) and the protonated forms ($APTS^+$, $EAPTS^+$, $PAPTS^+$) of the amines were considered, being contemporaneously present on the catalysts surface during the DMC synthesis. The intermediate, 2-hydroxyethyl methyl carbonate (HEMC), and its complexes with the amines were also considered. The deprotonated methanol (CH_3O^-) was also modeled to help the assignment of the IR spectra. All the systems have been optimized by a density functional based method, the Becke's three-parameters hybrid exchange functional [46] supplemented with the Lee, Yang and Parr's gradient-corrected correlation functional [47] (B3-LYP). All the elements have been modeled by means of the fully optimized triple-ζ valence basis sets proposed by Ahlrichs et al. [48] with polarization (TZVp). Geometry optimization has been carried out by means of the Berny optimization algorithm with analytical gradient. The thresholds were set to 0.000450 and 0.000300 a.u. for the maximum and the rms forces respectively; and to 0.001800 and 0.001200 a.u. for the maximum and rms atomic displacements, respectively. A (99,590) pruned grid was used (*i.e.* 99 radial points and 590 angular points per radial point). No symmetry constraints have been imposed. Electronic charges have been calculated by using the Mulliken population analysis. The binding energy (BE) of the complex constituted by the 2-hydroxyethyl methyl carbonate and the amine was calculates as the difference between the energy of the isolated moieties and the energy of the complex. Being the flexibility of the clusters larger in the gas phase than after grafting, the binding energy has been also estimated by excluding the contribution due to the deformation energy (BE_{def}). This quantity was also determined by single point calculations on the B3LYP geometries at the MP2 level [49] in the frozen-core approximation (BE_{defMP2}) in order to evaluate the role of the dispersion forces in the interaction.

Harmonic frequencies have been obtained by analytically determining the second derivatives of the energy with respect to the Cartesian nuclear coordinates and then transforming them to mass-weighted coordinates. No scaling factor has been adopted. The dissociation energy from the ground state (D_0) of the adducts was calculated from the corresponding dissociation energy from the potential energy minimum BE by including the zero point energies (ZPE) of reactants and products. The ZPE was calculated in the harmonic approximation. The enthalpy variations (D_{RT}) at standard conditions (298.15 K and 1 atm) were derived from the reaction energies including the ZPE and temperature corrections. The temperature corrections were computed using the standard expressions for an ideal gas in the canonical ensemble. No scaling factors were adopted.

All the energetic data have been corrected for the basis set superposition error (BSSE) following the a posteriori method proposed by Boys and Bernardi [50] as implemented in *Gaussian 09*. The BSSE corrected energetic values are signalized by a c superscript and were obtained from the computed Y values as $Y^c = Y - BSSE$.

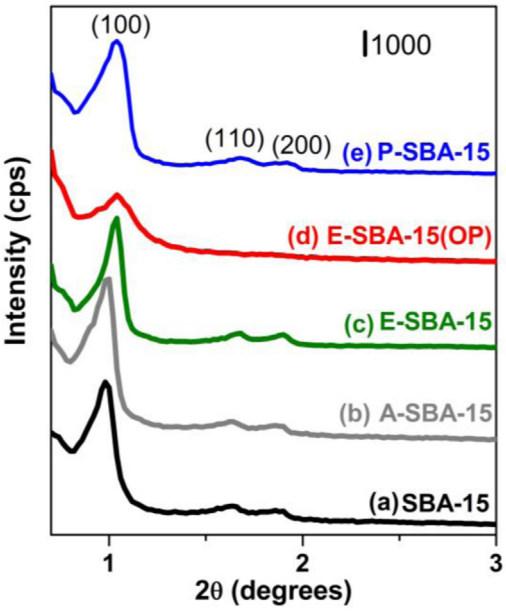

Fig. 1. Low-angle XRD patterns of pure SBA-15 (a, black) and of amino-modified A-SBA-15 (b, grey), E-SBA-15 (c, green), E-SBA-15(OP) (d, red) and P-SBA-15 (e, blue) samples.

3. Results and discussion

3.1. *Characterization of amino-modified SBA-15 catalysts*

The physico-chemical properties of the catalysts were evaluated by means of different characterization techniques: XRD, TG analysis, FT-IR spectroscopy, C-H-N elemental analysis and N_2 physisorption measurements at 77 K.

The low-angle XRD diffraction patterns of the amino-modified SBA-15 samples are reported in Fig. 1 and compared with the pattern of the pure SBA-15 silica.

The pure SBA-15 silica sample (Fig. 1, curve a) exhibits three well-resolved peaks at 0.9, 1.5 e 1.8° 2θ, indexed as (100), (110) and (200) planes and associated with the 2D hexagonal *p6 mm* symmetry typical of this mesoporous sample [51]. The amine-modified SBA-15 samples obtained by post-synthesis grafting (Fig. 1b–d curves) show the same reflections of the reference silica sample, proving that the grafting process did not affect the hexagonally ordered structure typical of the SBA-15 system.

FT-IR spectra reported in Fig. 2(A) provide a clear evidence of the presence of organic chains on the surface of the silica samples.

The IR spectrum of pure SBA-15 sample (Fig. 2(A), a) is characterized by the presence of the fingerprints of the siliceous framework. In particular, the absorptions at $\nu < 2100\ cm^{-1}$ can be attributed, on the basis of their spectral behaviour and of the literature [52], to the

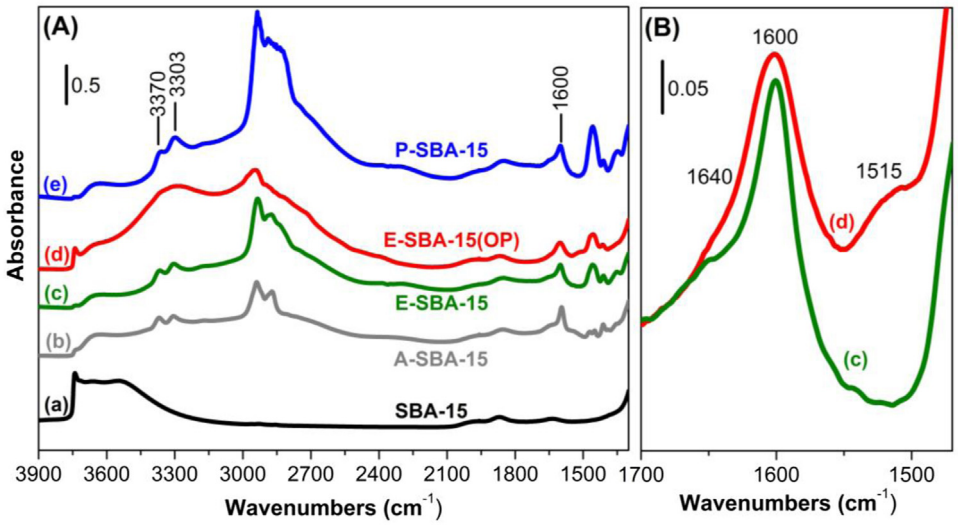

Fig. 2. Section (A): absorbance FT-IR spectra of plain SBA-15 (a,black) and of amino-modified A-SBA-15 (b, grey), E-SBA-15 (c, green), E-SBA-15(OP) (d, red) and P-SBA-15 (e, blue) samples after activation in vacuum at 150 °C for 2 h. Section (B) Magnification of the 1700–1470 cm^{-1} spectral range for E-SBA-15 (c, green) and E-SBA-15(OP) (d, red) samples.

Si—O—Si combination (overtones) modes. Still, the sharp signal at 3745 cm^{-1} is generated by the stretching modes of OH groups free from hydrogen bonding interactions, whereas the broad band in the 3800–3000 cm^{-1} range is related to the stretching vibrations of OH groups mutually interacting by hydrogen bonding [53]. The presence of the grafted organic moiety visibly modifies the spectrum of the bare SBA-15 system, producing a series of new complex absorptions generated by the alkylamine chains (Fig. 2(A), b, c, e spectra). In particular, in the spectra of modified systems, the stretching vibration associated to free OH groups at 3745 cm^{-1} disappears due to the consumption of the silanol groups by the alkoxysilane condensation reaction and, at the same time, new bands appear at 3370 and 3303 cm^{-1} and at 1600 cm^{-1}. These signals, ascribable to the asymmetric and symmetric stretching modes and to the scissoring mode of the NH_2 groups, are present in the spectra of all functionalized samples, proving the insertion of the desired amino group inside the SBA-15 channels.

The textural properties of all samples were determined by N_2 physisorption at 77 K. The N_2 adsorption-desorption isotherms and the pore size distribution of the materials are reported in Figs. S1 and S2 of the Supplementary material.

The adsorption isotherms of the pure SBA-15 and of all post-synthesis grafted samples are of type IV with an H1 hysteresis loop, typical of mesoporous materials with cylindrical pores. This isotherms profile proves that the ordered arrays of pores typical of the SBA-15 structure is retained also after the functionalization process [54]. The BET algorithm was used to estimate the specific surface area (SSA) of the solids. As reported in Table 1, the SSA and the pores volume decrease with the parallel increase of the alkylamine chain length, testifying that the grafting of the organic moieties was carried out inside the channels of the SBA-15 system. The pore size distribution (Fig. S2) was obtained by the NL-DFT model using the desorption branch of the isotherms. The pure SBA-15 system exhibits a narrow pore size distribution (85 Å) generated by the main channels of the mesoporous structure and a second family of smaller cavities of 20–40 Å diameter, ascribable to pores connecting the bigger mesopores. It is evident that all post-synthesis grafted samples possess just one predominant family of pores (maxima in the 70–80 Å range) corresponding to the main ordered mesoporous cavities of the SBA-15 silica. The smaller size of the main channels of the ordered silica structure testifies that the grafting of the desired amine moieties occurs inside the mesoporous silica cavities.

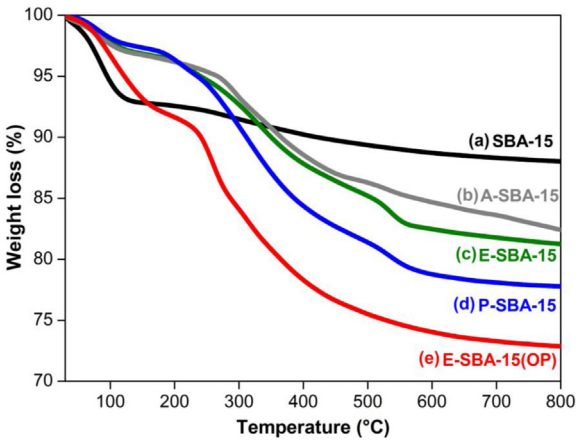

Fig. 3. TG curves, collected under O_2 flow, of pure SBA-15 (a, black) and of amine-modified A-SBA-15 (b, gray), E-SBA-15 (c, green), P-SBA-15 (d, blue) and E-SBA-15(OP) (e, red) samples.

The molar concentration of N atoms was estimated by elemental analysis and reported in Table 1. As expected, the N content (expressed as mmol of N per g of sample) increases passing from A-SBA-15 to P-SBA-15. The density of silane molecules, calculated using the molar concentration of nitrogen atoms, the specific surface of the bare SBA-15 and the number of N present in each silane chain, is similar for all samples (see Table 1, last column), due to the fact that the same molar concentration of organic silanes was used for the grafting procedure.

The thermogravimetric analysis was carried out to assess the thermal stability of the grafted amine moiety. The thermal profiles of post-synthesis grafted samples, reported in Fig. 3, exhibit three main weight losses: the first one, in the 35–130 °C range, due to the removal of all physisorbed water (this is the only step evident in the case of pure SBA-15), the second one, in the 180–450 °C range, generated by the first decomposition step of the organo-silane and the third one, in the 480–680 °C range, due to the complete removal of the organic species from the silica surface.

Table 1
Specific Surface Area (SSA), total pore volume (Vp), concentration and density of amino groups and silanes.

Catalyst	SSA [m^2/g]	Vp [cc/g]	Conc. N [mmol/g][a]	Density of N [n° N/nm^2][b]	Density of Silane [n° Silane chains/nm^2][c]
SBA-15	720	0.98	–	–	–
A-SBA-15	563	0.94	1.05	0.88	0.88
E-SBA-15	360	0.57	2.60	2.17	1.08
P-SBA-15	236	0.41	3.50	2.93	0.97
E-SBA-15(OP)	430	0.62	2.76	–	–

[a] Determined by elemental analysis.
[b] Calculated by dividing the number of N atoms by SSA of bare SBA-15.
[c] Obtained by dividing the density of nitrogen by the number of N atoms in the single chain of the silane.

The physico-chemical properties of the catalyst synthesized following the one-pot synthetic procedure were evaluated by means of the same characterization techniques employed for the post synthesis grafted materials. The low-angle XRD diffraction pattern of the E-SBA-15 (OP) sample (Fig. 1d) is characterized by the presence of a single and broad peak at *ca.* 0.9° 2θ, the (100) reflection, suggesting that the introduction of a silane with long chain, during the SBA-15 framework synthesis, leads to a material with a more disordered structure than purely siliceous SBA-15. It is impressive in this sense, the difference among the E-SBA-15 (OP) and E-SBA-15 patterns reported in Fig. 1. The decrease of the structural order during the one-pot grafting was already observed in the literature, employing short organo silanes such as aminopropyltrietoxysilane and vinyl-silane [55,56].

All the textural features of E-SBA-15(OP) are summarized in Table 1, together with the molar concentration of N atoms estimated by elemental analysis.

The concentration of N atoms of the E-SBA-15(OP) catalyst is perfectly comparable to the value calculated for the corresponding post synthesis grafted material (E-SBA-15). However, as demonstrated in the following, the grafted amine species are probably less homogeneously distributed in the one-pot synthesized material.

The N_2 adsorption-desorption isotherms and the pore size distribution of this material are reported in Figs. S1 and S2 of the Supplementary material. The one-pot sample is characterized by a SSA comparable to the value reported for its corresponding post-synthesis grafted material. Instead, for what concerns the N_2 isotherm, E-SBA-15(OP) sample shows a type IV profile with an H3 hysteresis loop, testifying a higher heterogeneity of the pore size [57]. In fact, this sample exhibits a broader pore size distribution (see Fig. S2 in Supplementary material, red curve) with respect to the post-synthesis grafted materials, with pores in the 30–90 Å range. The heterogeneity of the pores families in the E-SBA-15(OP) is derived from a less structural organization of this material, in agreement with the XRD analysis, and, probably, also from a largely heterogeneous distribution of the organic functionalities [58].

The FT-IR spectrum of the E-SBA-15(OP) catalyst is reported in Fig. 2(d, red) in comparison with the spectrum of the corresponding post-synthesis grafted material E-SBA-15 (c, green). It is evident that, in the case of the E-SBA-15(OP) sample, a fraction of the amino groups is clearly protonated as highlighted, in the magnified spectral section of Fig. 2(B), by: (i) the evident broader profile of the band at 1600 cm^{-1} related to the scissoring mode of the NH_2 group (indicating the existence of an overlapped signal at ~1640 cm^{-1}, ascribable to the asymmetric NH_3^+ deformation); (ii) the presence of an additional band at 1515 cm^{-1} associated to the symmetric NH_3^+ bending mode [59].

The TG profile of the E-SBA-15(OP) sample (Fig. 3e) highlights some differences with respect to the other family of samples. In particular, the more pronounced weight loss step, in the 200–450 °C range, is probably related to two different decomposition phenomena: the thermal degradation of both the alkylamine chains and the residual organic templating agent (employed in the synthesis of the mesoporous silica), not completely removed during the extraction step with ethanol.

Summarizing, although the one-pot synthetic pathway seems to be an easier method for the preparation of amino-functionalized SBA-15 catalysts, two main problems were highlighted: (i) the inclusion of the organic moiety during the SBA-15 structure formation leads to less homogeneous distribution of the grafted alkylamine chains; (ii) the use of acid conditions during the synthesis (to help the silica precursor hydrolysis) causes the protonation of a significant fraction of the available amino groups. It is worth noting that the deprotonation of these amino groups can occur only with strong basic treatments that, at the same time, can damage the ordered structure of the SBA-15 silica (results not shown for the sake of brevity).

3.2. Transesterification reaction of EC with methanol: catalytic tests

The catalytic behaviour of all amino-modified SBA-15 samples was evaluated with preliminary experiments at 65 °C and atmospheric pressure (see Fig. 4).

The E-SBA-15 sample displays the highest catalytic activity, with a relatively high DMC yield (around 17%). In these particular reaction conditions and in the presence of this catalyst, a high yield (around 40%) of the reaction intermediate, 2-hydroxyethyl methyl carbonate (HEMC) is also observed. In contrast, the corresponding one-pot material (E-SBA-15(OP)) exhibits null catalytic activity. For what concerns the A-SBA-15 and P-SBA-15 materials, they reveal a similar conversion of EC (58 and 54% respectively). However, in this case, the yield of DMC is almost null, despite the relatively high EC conversion, whereas a high selectivity towards the reaction intermediate is observed (around 55%), indicating that the reaction stops with the HEMC formation in both cases.

The results of the preliminary catalytic tests at 65 °C demonstrated that only the system grafted with the EAPTS chain is able to partially convert EC into DMC. In contrast, in the presence of both APTS and PAPTS groups, the reaction stops at the HEMC formation. The peculiar catalytic results obtained at 65 °C can be probably related to the stabilization capacity of the reaction intermediate from the different alkylamine chains that, at this temperature, can allow or not the second CIR between HEMC and methanol to yield DMC.

Due to its higher catalytic activity, we decided to study more in detail the E-SBA-15 catalyst, performing the reaction in a stainless steel autoclave reactor, by maintaining the same ratio of the reagents mixture and the catalyst as for the previous test but pressurizing the vessel at 10 bar pressure of nitrogen. The catalytic results, as a function of the reaction temperature, are reported in Fig. 5. No test has been carried out over 140 °C in order to avoid the decomposition of the amine moiety (see TG measurements in Fig. 3).

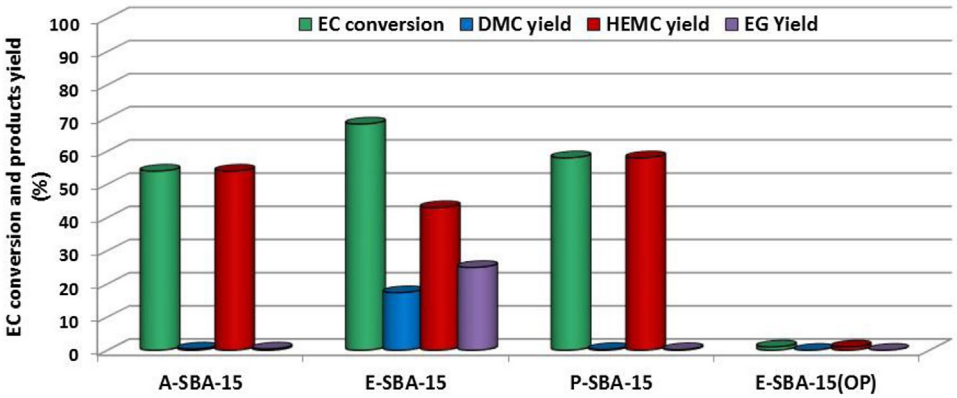

Fig. 4. Catalytic results: CH_3OH:EC = 10:1, T = 65 °C, t = 6 h, p = 1 bar, catalyst 5% w/w with respect to EC. EC conversion (green), DMC yield (blue), intermediate (HEMC) yield (red) and EG yield (violet). The catalytic data (conversions and yields) are reported for each sample in the order shown in the legend. (For interpretation of the references to colour in this figure legend, the reader is referred to the web version of this article.)

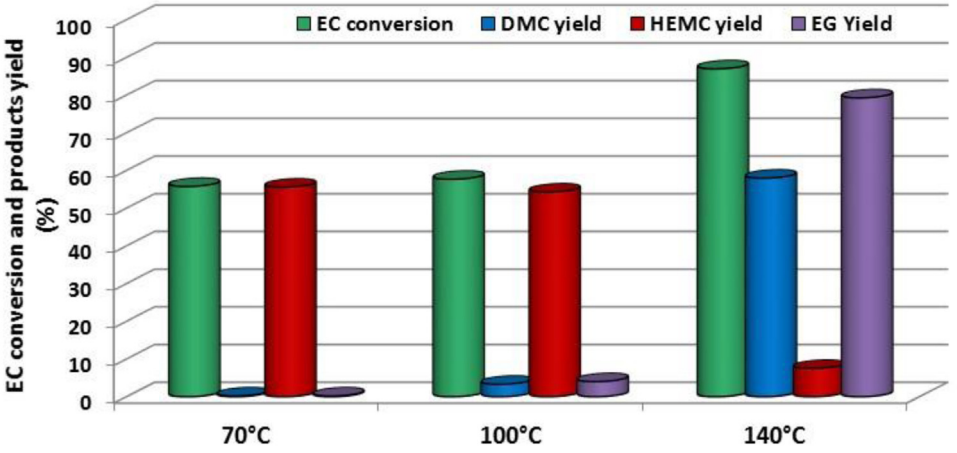

Fig. 5. Catalytic results as a function of the reaction temperature, CH_3OH:EC = 10:1, t = 6 h, autoclave reactor purged with 10 bar of nitrogen, catalyst E-SBA-15, 5% w/w with respect to EC. EC conversion (green), DMC yield (blue), intermediate (HEMC) yield (red) and EG yield (violet). The catalytic data (conversions and yields) are reported for each sample in the order shown in the legend. (For interpretation of the references to colour in this figure legend, the reader is referred to the web version of this article.)

It is clear that until 100 °C the EC conversions are similar and the DMC yield is extremely low, whereas the selectivity to HEMC is very high. The very similar EC conversions observed at both 70 and 100 °C can be explained considering that the first CIR is a thermodynamically equilibrium limited reaction, that, at relatively low temperature, is probably more affected by the molar ratio between the two reagents (in particular the methanol excess), rather than by a temperature increase of 30 °C. Above 100 °C, the situation completely changes. In fact, a yield of DMC as high as 58% can be observed at 140 °C. At the same time, the yield of asymmetric intermediate drastically decreases, demonstrating that the second carbonate interchange reaction (CIR) between HEMC and methanol to yield DMC requires higher temperatures to proceed.

On the other hand, at higher temperature, the contribution of EC decomposition to EG becomes relevant, with an increase of the gap between the EC conversion and the sum of the products yields.

Considering the good catalytic performances of E-SBA-15, the EC conversion and the products distribution have been investigated also as a function of the reaction time, performing the reaction at 140 °C in the autoclave and analyzing the mixture at different times (see Fig. 6).

The kinetic curves reported in Fig. 6 clearly confirm the role played by the HEMC as reaction intermediate. In fact, the yield of HEMC reaches its maximum after 1 h and then it gradually decreases for higher reaction times, with the parallel formation of the reaction products, DMC and EG. As expected, the two products form in equimolar amount until 2 h of reaction then, for higher reaction time, the contribution of the EC decomposition clearly emerges and the EG yield rises above the DMC yield.

In order to verify the recyclability of the E-SBA-15 catalyst, recycle tests were carried out and the reaction was performed many times using the same catalyst (see Figs. 7 and S3).

After each reaction run, the mixture was analyzed and the catalyst recovered by filtration, washed with acetone and dried overnight at 120 °C. Interestingly, no catalyst deactivation can be observed at least for four consecutive catalytic cycles, proving the extremely high stability of the E-SBA-15 catalyst in the optimized reaction conditions.

The stability of the amino groups grafted to the E-SBA catalyst has been evaluated performing a leaching test in the optimized reaction conditions. In particular, the leaching of the organic chains containing the basic amino groups was investigated stopping the reaction after 2 h, and separating the catalyst by hot filtration. After that, the liquid mixture without catalyst was charged in the autoclave again, purged with 10 bar of nitrogen and heated again to the selected temperature (140 °C). These results, reported in Fig. S4 of the Supplementary material, clearly show that, after the removal of the catalyst, the conversion of EC continues to increase. However, this increase is only due to the parasite decomposition reactions that directly lead to the formation of EG. The yield of DMC is com-

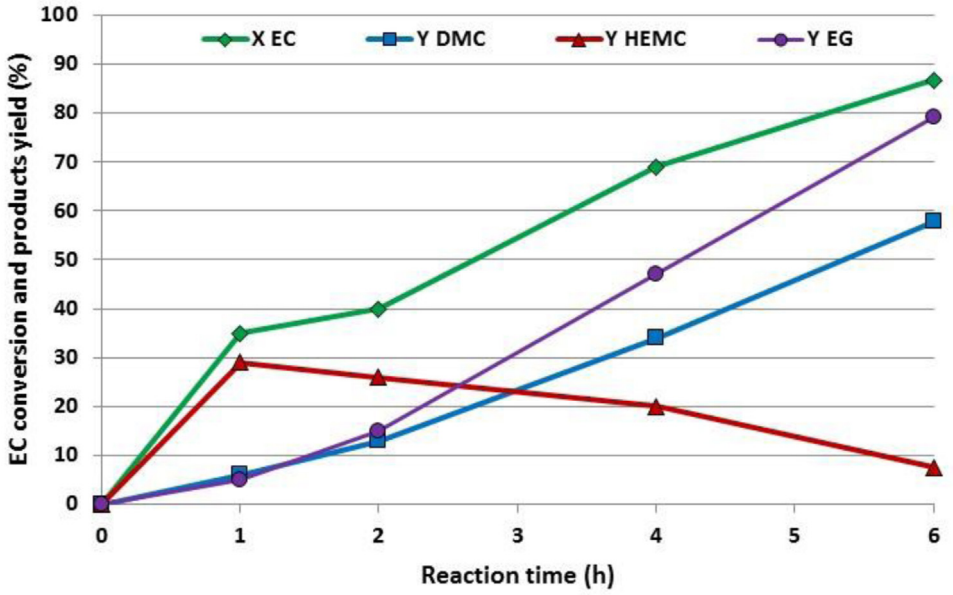

Fig. 6. Catalytic results as a function of the reaction time. CH_3OH:EC = 10:1, T = 140 °C, t = 6 h, autoclave reactor purged with 10 bar of nitrogen, catalyst E-SBA-15, 5% w/w with respect to EC. EC conversion (green), DMC yield (blue), intermediate (HEMC) yield (red) and EG yield (violet). (For interpretation of the references to color in this figure legend, the reader is referred to the web version of this article.)

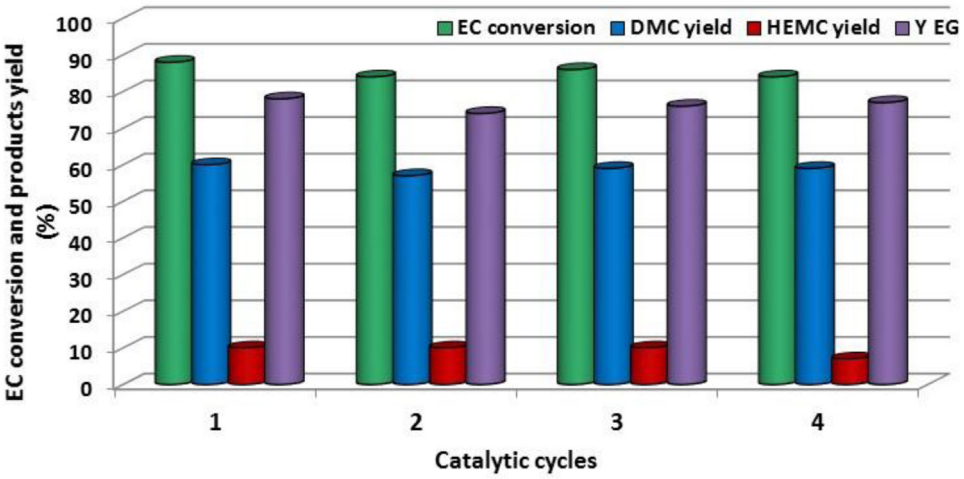

Fig. 7. Recycle tests of E-SBA-15. CH_3OH:EC = 10:1, T = 140 °C, t = 6 h, autoclave reactor purged with 10 bar of nitrogen, catalyst E-SBA-15, 5% w/w with respect to EC. EC conversion (green), DMC yield (blue), HEMC yield (red) and EG yield (violet). The catalytic data (conversions and yields) are reported for each sample in the order shown in the legend. (For interpretation of the references to color in this figure legend, the reader is referred to the web version of this article.)

pletely unaffected by the catalyst filtration confirming the higher stability of the symmetric carbonate compared to the asymmetric HEMC, whose yield drops to 1%.

This test proves that the E-SBA-15 catalyst is stable in the selected reaction conditions with no leaching of the active basic groups. A possible leaching of the grafted amino groups, in fact, would lead to the homogenous catalyzed CIR with methanol, with the resulting increase of the DMC yield also after the catalyst removal.

The reaction has been studied in the optimized reaction conditions (140 °C and 6 h) for all post-synthesis grafted materials: the catalytic results are compared in Fig. 8. These catalytic tests were not carried out in the presence of the E-SBA-15(OP) material, due to the virtually null catalytic activity exhibited by this sample in the preliminary tests.

It is noteworthy that, in these reaction conditions, the EC conversion is the same (around 87%) for all catalysts, due to the thermodynamic equilibrium of the reaction. Moreover, the A-SBA-15 catalyst exhibits the lower selectivity, with a higher degradation of the reagent and a lower DMC yield (around 25%), whereas the catalysts grafted with longer amine chains lead to similar catalytic behaviours, with definitely higher yield of DMC (around 58%) and a slightly lower decomposition of EC to EG. It is worth noting that the P-SBA-15 catalyst exhibits a higher HEMC yield with respect to the E-SBA-15 sample, whereas, for these two materials, the DMC yields are perferctly comparable. In all cases, at 140 °C, the yield of the reaction intermediate (HEMC) is much lower with respect to the reaction carried out at 65 °C, demonstrating the close correlation between the reaction temperature and the occurrence of the second CIR between HEMC and methanol to yield DMC. At this temperature, in fact, the mobility of the intermediate species is probably higher and, therefore, the second CIR is no more related to the HEMC stabilization capacity from the alkylamine chains.

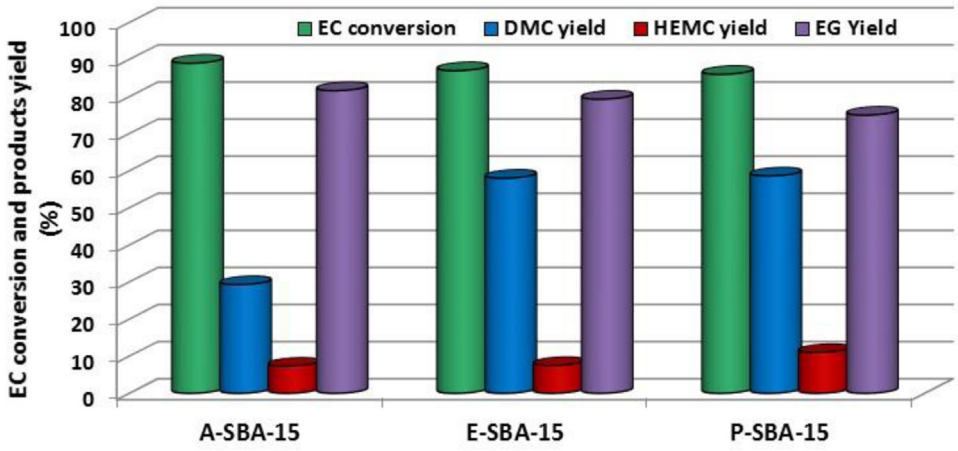

Fig. 8. Catalytic results, CH_3OH:EC = 10:1, T = 140 °C, t = 6 h, autoclave reactor purged with 10 bar of nitrogen, catalyst 5% w/w on the respect of EC. EC conversion (green), DMC yield (blue), HEMC yield (red) and EG yield (violet). The catalytic data (conversions and yields) are reported for each sample in the order shown in the legend. (For interpretation of the references to color in this figure legend, the reader is referred to the web version of this article.)

The turn-over-number (TON), referred to both the number of N atoms and the number of silane chains, was calculated and reported in Table S1 of the Supplementary material. It was found that comparing the TON in mild conditions (entries 1–3), *i.e.* at 65 °C and atmospheric pressure, the number of N atoms of the silane chains does not affect the activation of the reactants and the formation of the products. In fact, the TON referred to the N atoms (TON^a) decreases by increasing the number of N atoms, whereas it is similar for all samples if calculated with respect to the number of silane chains (TON^b). In other words, only the primary amine group $-NH_2$ seems to be involved in the reactants activation to yield HEMC, the main reaction product at mild conditions. However, when the TON is calculated under more severe conditions (entries 4–6), *i.e.* at 140 °C and at 10 bar pressure of nitrogen, the presence of other N atoms on the silane chains seems to affect the reactant and intermediate activation. This is proved by the decrease of the TON^a and by the increase of the TON^b, when the number of N atoms on the alkylamine chain is increased. However, these variations are much more pronounced passing from the material with one N atom in the alkylamine chain (A-SBA-15) to the material with two N atoms (E-SBA-15) and less evident passing from E-SBA-15 sample to the catalyst with three N atoms in each silane chain.

From the data collected in the optimized reaction conditions (at 140 °C and at 10 bar pressure of nitrogen), it can be derived that passing from APTS to EAPTS, *i.e.* increasing the number of basic amino groups on the silica surface, the catalytic performances of samples are enhanced. Nevertheless, by using SBA-15 sample functionalized with PAPTS (and containing the highest concentration of N species) just a slight improvement of the catalytic activity can be observed, especially for what concerns the DMC yield. Moreover, results obtained at higher temperature highlight the importance of preventing the direct decomposition of EC to EG, which occurs through either decarboxylation (or decarbonylation) or hydrolysis.

The catalytic results clearly highlight the absence of a specific correlation between the catalysts activity and their textural properties (specific surface area, pore volume and pore size distribution). In fact, it is clear that the material possessing a definitely higher specific surface area and pore volume (A-SBA-15) displays the lower catalytic activity both at low and high temperature, whereas both the materials with lower specific surface area and pore volume (E-SBA-15 and P-SBA-15) possess an enhanced catalytic activity especially at high temperature. For this reason, we decided to employ FTIR spectroscopy and theoretical calculations to find a correlation between the catalytic performances and other catalyst features, such as the reagents activation capacity or the ability to stabilize the intermediate from alkylamine chains of different nature.

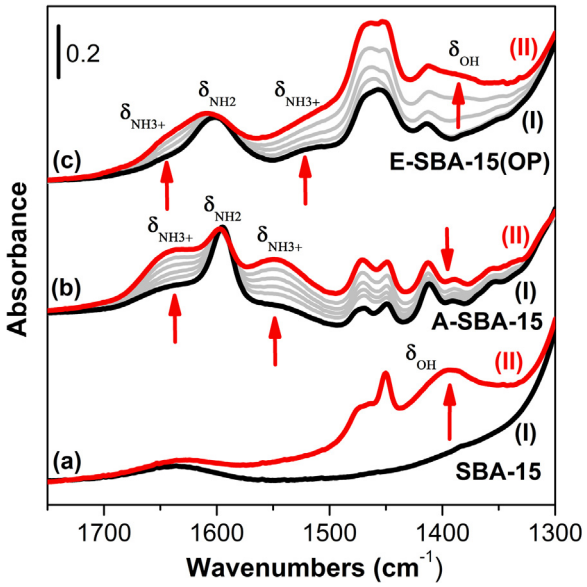

Fig. 9. Absorbance FT-IR spectra, in the 1800–1300 cm^{-1} spectral range, of SBA-15 (set a), A-SBA-15 (set b) and E-SBA-15(OP) (set c) after activation in vacuo at 150 °C (I, black spectra), after contact with 40 mbar of methanol vapours at BT (II, red spectra) and after gradual methanol evacuation at BT till to 2 h (light grey spectra). (For interpretation of the references to color in this figure legend, the reader is referred to the web version of this article.)

3.3. In-situ *IR study of methanol activation over amino-modified SBA-15*

The interesting catalytic behaviour of these systems was further investigated by means of *in situ* IR spectroscopy in order to study the step of methanol activation in the presence of amino-modified catalysts and to highlight the importance of this step in the whole catalytic cycle.

Fig. 9 compares the effect of 40 mbar equilibrium pressure of methanol vapours in contact with SBA-15 (a), A-SBA-15 (b) and E-SBA-15(OP) (c). The assignment of the vibrational frequencies of the A-SBA-15 spectra made on the basis of literature data and

Table 2
Experimental vibrational frequencies of the A-SBA-15 system in the 1700–1500 cm^{-1} and their assignment based on the calculations at B3-LYP/TZVp level on the APTS, $APTS^+$ and MeO^- clusters. The corresponding calculated normal modes are also reported for comparison.

Frequency exp. (cm^{-1})	Frequency calc. (cm^{-1})[b]	Cluster	Assignment
1639	1671	$APTS^+$	$-NH_3^+$ as. bending
1602(s)[a]	1664	$APTS^+$	$-NH_3^+$ as. bending
1594	1663	APTS	$-NH_2$ scissoring
1549	1517	$APTS^+$	$-NH_3^+$ sym. bending
1450	1523	MeO^-	$-CH_3$ sym. bending
1460	1521	APTS	$-CH_2$ scissoring
1528	1510	$APTS^+$	$-NH_3^+$ sym. bending

[a] s = shoulder.
[b] No scaling factor has been adopted.

of the calculations is reported in Table 2. A discussion aimed to the comparison between the experimental and theoretical values is reported in Section S5 of the Supplementary material.

The spectra collected after the activation of the materials are reported in black (I) in the 1800–1300 cm^{-1} spectral range. For what concerns the bare SBA-15 sample, after the contact with methanol vapours (see red spectrum (II), spectral set (a), Fig. 9), an envelope of bands appears in the 1500–1300 cm^{-1} spectral range. In particular, the bands at 1460 and 1450 cm^{-1} are generated by the bending vibrations of the $-CH_3$ unit, whereas the broad signal located at ~1400 cm^{-1} can be ascribed to the bending vibrational mode (δ_{OH}) of methanol $-OH$ moiety [59]. Moreover, observing the spectrum of the plain SBA-15 in the 3900–2800 cm^{-1} range after the contact with methanol, it is evident that the ν_{OH} spectral region appears strongly perturbed (see Fig. S5 in the Supplementary material). In particular, the signal ascribable to the free OH species at 3740 cm^{-1} (see black spectrum, Fig. S5 in Supplementary material) totally disappears and, at the same time, a broad and unresolved band envelope appears at 3700–3000 cm^{-1} (see red spectrum, Fig. S5 in Supplementary material). All these spectral modifications highlight that methanol simply interacts with the pure SBA-15 system, giving rise to weak H-bonding interactions with its surface OH-groups. On the contrary, in the presence of A-SBA-15 sample, methanol undergoes deprotonation generating the corresponding alcoholate (CH_3O^-). This phenomenon is clearly evident in the spectral set (b) of Fig. 9 relative to the A-SBA-15 system. After the activation process (black spectrum, I), the spectrum is dominated by the band located at 1594 cm^{-1} ascribable to the NH_2 scissoring mode (δ_{NH2}) of the amino group grafted to the silica surface. Moreover, the weak absorption bands at 1639 and 1549 cm^{-1} are ascribed to the asymmetric and symmetric δ_{NH3+} vibrations respectively, indicating the presence in the starting material of a small fraction of amino groups in the protonated form. The signals between 1500 and 1400 cm^{-1} can be ascribed to the CH_2 bending vibrations of the amino-propyl chain. The contact with methanol (red spectrum, II) leads to a slight enlargement of the band at ~1600 cm^{-1} (NH_2 deformation) and to the parallel increase of the NH_3^+ bands (1639 and 1549 cm^{-1}). No band ascribable to the δ_{OH} mode of methanol molecule is present in the spectrum at around 1400 cm^{-1}. These spectral modifications are indicative of the dissociative adsorption of methanol to form the alcoholate species (CH_3O^-) with the parallel amine protonation. In this view, a strong decrease of the intensity of the band at 1600 cm^{-1} related to $-NH_2$ group is expected, whereas only a slight enlargement is observed. This fact can be explained by the calculations, indicating that, in the protonated amine, two asymmetric bending modes related to the $-NH_3^+$ group are present, one of them only slightly different from the bending mode of the $-NH_2$ group (see Table 2).

A similar spectral behaviour could be observed after the contact of methanol with both E-SBA-15 and P-SBA-15 samples (results not shown for the sake of brevity).

For what concerns the one-pot catalyst (E-SBA-15(OP)), the contact with 40 mbar of methanol produces two opposite situations (see red spectrum (II) of spectral set (c) in Fig. 9): (i) a fraction of methanol undergoes deprotonation to form the CH_3O^- species as highlighted by the increase of the bands ascribable to the asymmetric and symmetric NH_3^+ deformation (at 1640 and 1516 cm^{-1} respectively); (ii) the presence of the broad signal at ~1400 cm^{-1} due to the δ_{OH} mode of methanol points out that this catalyst is not able to convert all methanol molecules into the corresponding alcoholate. The particular behaviour of the E-SBA-15(OP) catalyst can be explained by taking into account the not homogeneous distribution of the grafted alkylamine chains and the presence of a consistent fraction of the protonated amino groups already formed during the synthesis.

Moreover, for both A-SBA-15 and E-SBA-15(OP) samples, the formation of the CH_3O^- species and of the corresponding protonated amine ($APTS^+$ or $EAPTS^+$) is a completely reversible phenomenon. In fact, the spectra of the samples just after the activation process (black curves, I) are totally restored after a simple evacuation at BT (see light grey spectra). It is interesting to notice that the calculations indicate that the proton affinity of methanol would be larger than for amines. In fact, optimization of the protonated amine/CH_3O^- couple ended to the corresponding neutral amine/CH_3OH couple. This result would, on one hand, explain the reversibility of the $CH_3OH \leftrightarrows CH_3O^-$ transformation observed experimentally and, on the other hand, it evidences the important role of neighbor surface species, not considered in the models, in stabilizing the polar pair in the real catalyst.

Considering the data reported in the catalytic section and the results of the spectroscopic investigation, it is possible to state that the dissociative adsorption of methanol has to be considered the key step of the whole catalytic cycle. In fact, as demonstrated by the catalytic results, the E-SBA-15(OP) material, containing a consistent fraction of protonated alkylamine chains, is not able to catalyze the first CIR between EC and methanol. All the other catalysts, instead, are able to form the CH_3O^- species that, in turn, can attack the EC molecule and lead to the formation of the reaction intermediate (HEMC).

3.4. The reaction intermediate (HEMC) and its stability in the presence of different amino-modified SBA-15 systems

From the catalytic results it can be hypothesized that the interaction strength between the intermediate and the alkylamine chains of the catalyst plays an important role in driving the reaction. Yang et al. [16] reported about the transesterification of EC with methanol over a series of DABCO-based ionic liquids with different anions, achieving good DMC yields and selectivities, especially for the catalysts containing the OH^- anion. These authors investigated the effect of the various anions on the catalyst performances. In particular, they found that the reaction intermediate (HEMC) was the

only product in the case of the catalyst containing the BF_4^- anion. Therefore, in this case, the reaction stopped at the HEMC formation. This peculiar catalytic result can be related to the stabilization capacity of the reaction intermediate due to the high Lewis basic character of the catalyst. In the presence of the BF_4^- anion, in fact, the lone electron pair on the N atom of the DABCO system is more prone to interact with the just formed intermediate, contributing to its excessive stabilization. The results reported by Yang et al. prove that the intermediate stabilization capacity is, after the dissociative adsorption of methanol, another important key factor that has to be considered in the choice of the proper catalytic system, in order to allow the HEMC species to undergo nucleophilic attack and to form the desired final product (DMC).

About that, an *in situ* FT-IR investigation of the reaction between EC and methanol, in the presence of our different active catalysts, has been carried out together with a theoretical study of the HEMC and of its complexes with the various amines (in both neutral or protonated forms), in order to correlate the capacity to stabilize the reaction intermediate with the catalytic performances of the material.

3.4.1. In situ *FT-IR study*

The FT-IR spectra collected in the 1900–1650 cm^{-1} spectral range at the various reaction steps are reported in Fig. 10. The *in situ* experiment has been carried out in controlled atmosphere at beam temperature (around 50 °C), as reported in the experimental section.

After activation in vacuum at 150 °C (a, black spectra), EC was sublimated on the catalysts (b, blue curves). The presence of the adsorbed EC was shown by the appearance of a doublet of bands at 1807 cm^{-1} and 1777 cm^{-1}, attributed to the combined stretching modes (ν_{CO}) of the carbonyl moiety. The doubling of this band is due to a Fermi resonance effect: the C=O stretching vibration interacts with the first overtone of the skeletal breathing vibration to give rise to two bands of approximately equal intensity [60]. When methanol vapours are introduced into the cell, the signals of EC immediately start to decrease and, at the same time, two new bands appear at around 1750 and 1700 cm^{-1} and gradually increase in intensity (see light grey and red (a) spectra). In particular, the signal located at 1750 cm^{-1} reaches the highest intensity after 1 h of reaction (see red spectra).

Taking into account the experimental conditions in which the reaction is carried out inside the IR cell (similar to the reaction conditions of the catalytic tests at 65 °C), it is possible to ascribe the signals at around 1750 cm^{-1} to the carbonyl stretching mode of the HEMC intermediate in interaction with the catalyst alkylamine chains. The experimentally observed frequencies of the HEMC carbonyl stretching mode (ν_{CO}) are reported in Table S2 of the Supplementary material and compared with the theoretical values calculated for the intermediate complexes with both neutral and protonated amines (the optimized geometries of these complexes are reported in Figs. 11 and S9 respectively, whereas some relevant energetic, structural and vibrational features are reported in Table S2).

The theoretical values calculated for the intermediate in interaction with the neutral amines are in good agreement with the experimental data. In particular, it is possible to observe that, for E-SBA-15 and P-SBA-15, the experimental bands related to the carbonyl stretching mode of the HEMC are shifted to lower frequencies (at 1753 cm^{-1} for E-SBA-15 and at 1751 cm^{-1} for P-SBA-15) with respect to the A-SBA-15 system (1755 cm^{-1}). A possible explanation of this shift, on the basis of the calculations, could be that the carbonyl group of the intermediate does not interact directly with the alkylamine chain in the presence of APTS, whereas a direct interaction between the carbonyl moiety and the —NH group of the amine can be observed in the presence of both EAPTS and PAPTS (see Fig. 11).

The intense band at 1700 cm^{-1} that appears in parallel to the signal at 1750 cm^{-1} (see red (a) spectra) is ascribable to the carbonyl stretching mode of a polymeric by-product (probably a poly-ether-carbonate) that can form in basic environment, in this particular *in situ* experiment, from the EC ring opening polymerization (see Scheme 4) [61,62]. It is worth noting that the higher is the basicity of the catalyst, the higher is the amount of formed by-product.

Considering the asymmetric spectral profile of the band at 1700 cm^{-1}, it is possible to state that also a normal mode due to the carbonyl stretching of the intermediate combined with a bending vibration of the $-NH_3^+$ group on the protonated amine could contribute to this signal, as shown by the calculations (see Table S2).

Fig. S6 of the Supplementary material displays the evolution of the reaction between EC and methanol for contact times exceeding one hour. After one hour of reaction (light grey spectra), the ν_{CO} stretching mode of the HEMC at ~1750 cm^{-1} decreases in intensity together with the bands of residual EC, at 1807 cm^{-1} and 1777 cm^{-1}, whereas the signal at 1700 cm^{-1} dramatically increases. These spectral changes have been monitored until 20 h of reaction (green spectra (d) of Fig. S6). After this period, the band at ~1750 cm^{-1} totally disappears, except for the P-SBA-15 system, whereas the signal at lower frequency (~1700 cm^{-1}) dominates the whole spectrum. These spectral changes indicate that, for high contact time with the catalysts, EC undergoes ring opening polymerization probably reacting also with the just formed HEMC in deprotonated form, producing a polycarbonate species, as reported in Scheme 4. It is interesting to note that, just for the P-SBA-15 sample, a fraction of HEMC does not react with EC to give the polymeric by-product, as testified by the presence of the signal at 1751 cm^{-1} even after 20 h of reaction (green spectrum (d) of P-SBA-15 spectral set in Fig. S6). This phenomenon could be explained considering a higher stability of the intermediate in the presence of the material grafted with the PAPTS chain that partially prevents the side reaction of the HEMC with EC.

The formation of these heavy by-products can be observed only in these particular reaction conditions.

3.4.2. *Computational study of the reaction intermediate stability*

Taking into account the basic strength of the alkylamine chains (APTS < EAPTS < PAPTS, see also Section S5), the catalytic activity of the materials would be expected to increase in this order: A-SBA-15 < E-SBA-15 < P-SBA-15. However, the catalytic behavior observed for the three grafted materials in the preliminary catalytic tests at 65 °C does not follow this trend. In the presence of A-SBA-15 and P-SBA-15, the reaction stops to HEMC, whereas only over E-SBA-15 a not negligible amount of DMC forms. These catalytic differences can be most likely due to the different stabilization of the HEMC by the various amines. A theoretical study of the HEMC complexes with both neutral and protonated amines (see Figs 11 and S9 and Table S2) allows explaining the catalytic performances of the materials.

Indeed, on the basis of the calculations, for the neutral amines, the stabilization of the intermediate on the catalyst surface does not follow the one expected on the basis of the increasing basicity of the amines (P-SBA-15 > E-SBA-15 > A-SBA-15), but it is A-SBA-15 > P-SBA-15 > E-SBA-15 (see BE^c_{defMP2} in Table S2). The unexpected stabilization of the intermediate in the case of APTS would be related to the involvement of surface silanols that would strongly contribute to the stabilization of the complex. In fact, due to the shorter length of the APTS chain, the carbonyl group of HEMC in the corresponding complex can interact with the terminal silanols (simulating surface silanols) causing an increase in the BE of about 20 kJ mol^{-1} in the considered clusters, that is of about the 50% of the

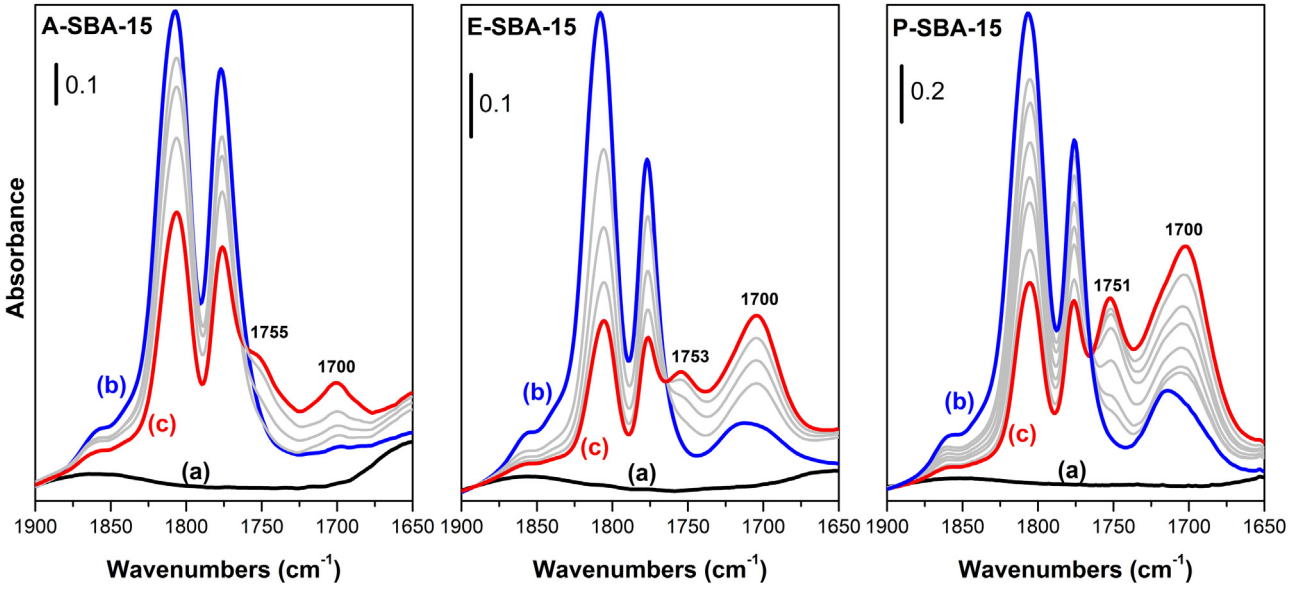

Fig. 10. Absorbance FT-IR spectra at BT, in the 1900–1650 cm^{-1} spectral range, of A-SBA-15, E-SBA-15 and P-SBA-15 after activation in vacuo at 150 °C (a, black spectra), contact with ethylene carbonate (b, blue spectra), and admission of 40 mbar of methanol: spectra recorded in time (light grey spectra) up to 1 h of contact (c, red spectra). (For interpretation of the references to color in this figure legend, the reader is referred to the web version of this article.)

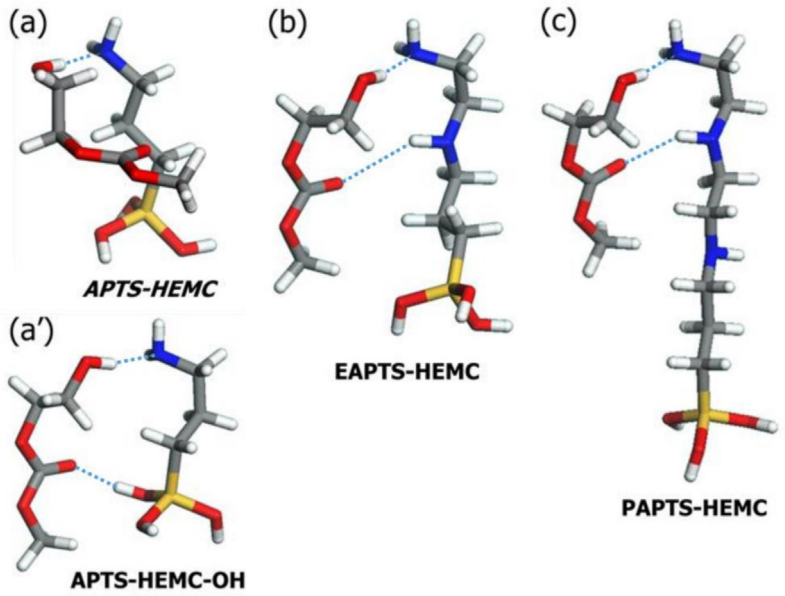

Fig. 11. Optimized geometries of the HEMC complexes with the organic amines in their neutral form as calculated at the B3-LYP/TZVp level. The C (grey), H (white), Si (yellow), O (red) atoms are represented with a stick style. The label of local minima structures is written in italics. (For interpretation of the references to color in this figure legend, the reader is referred to the web version of this article.)

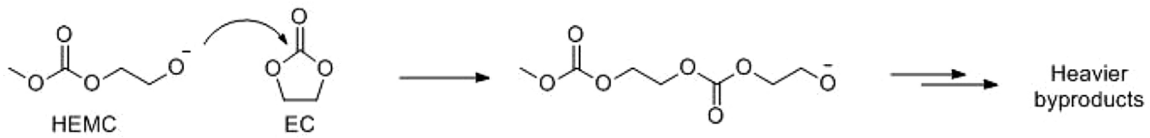

Scheme 4. Polymeric by-products formation.

energy (see BE^{c}_{defMP2} for APTS-HEMC and APTS-HEMC-OH in Table S2). In contrast, due to the longer chain length, a similar contribution is expected to be less important for E-SBA-15 and P-SBA-15. In fact, in the EAPTS-HEMC and PAPTS-HEMC models, the HEMC prefers to coordinate to the —NH group of the amine than with the Si-OH group.

Considering the intermediate complex as the transition state, the catalytic activity is then expected to be: E-SBA-15 > P-SBA-15 > A-SBA-15, *i.e.* inversely proportional to the stabilization

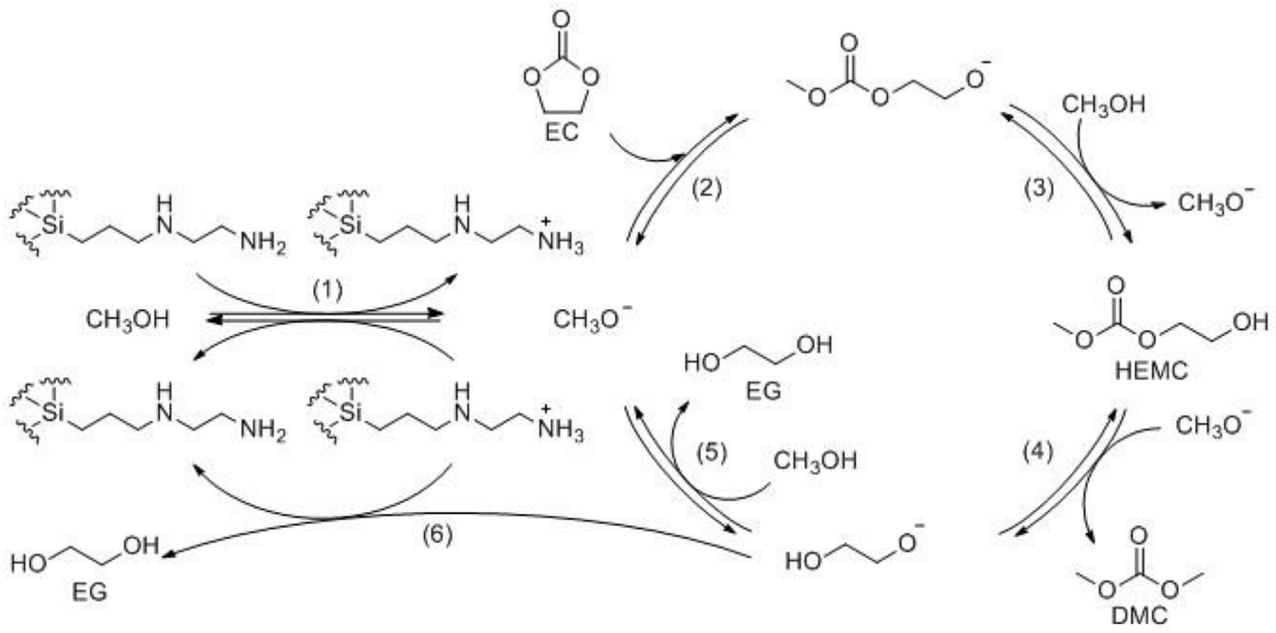

Scheme 5. Proposed mechanism for DMC formation over E- SBA-15 catalyst.

capacity of the intermediate. This conclusion allows to explain the results of the catalytic tests at 65 °C and atmospheric pressure: (i) in the presence of A-SBA-15 the reaction stops to the HEMC formation because the intermediate is overly stabilized by the parallel interaction with the APTS chain and a surface silanol; (ii) the P-SBA-15 system also excessively stabilizes the intermediate and does not allow the second CIR to occur; (iii) the E-SBA-15 catalyst with the lower stabilization of the intermediate, is able to catalyze both the CIRs yielding DMC.

The situation completely changes if the reaction is carried out at 140 °C. At this temperature, in fact, the higher mobility of the intermediate drives the reaction in a completely different way: the HEMC yield is very low and, at the same time, essentially DMC forms. Still, the catalytic activity of A-SBA-15 is lower, whereas E-SBA-15 and P-SBA-15 exhibit very similar catalytic performances.

This catalytic behaviour could be explained in different ways: (i) the basicity of the APTS chain could not be sufficient to obtain high yield in DMC; however, increasing the basic strength over a specific value the situation does not change anymore; (ii) the high stabilization of the intermediate in the presence of the APTS/OH couple could limit the catalytic activity of the A-SBA-15 system; (iii) the presence of a NH_2/NH couple in the same alkylamine chain could allow obtaining good yield in DMC. Moreover, it was clear from the calculations that HEMC is not able to interact with more than 2 N atoms per time. This would explain the very similar catalytic activity observed for E-SBA-15 and P-SBA-15 at 140 °C.

Considering the interaction between the intermediate and the protonated amines (see Fig. S9 and Table S2) a higher interaction energy is obtained due to the positive charge on the amine. It is possible to observe that, also for what concerns the protonated amines, the interaction with surface silanols is more likely for $APTS^+$ than for the other amines. In this case, the intermediate binding energies order follows this trend: $EAPTS^+ > PAPTS^+ > APTS^+$. The higher affinity towards the intermediate with respect to the neutral corresponds to a higher stabilization of HEMC and then a lower tendency to continue the reaction path. For what concerns this last point, it is interesting to notice that in the case of the catalytic tests at 140 °C, a fraction of HEMC does not convert to DMC. This fraction of intermediate could be interacting with the amines in the protonated form and, therefore, could not be able to undergo the second CIR.

3.5. Proposed reaction mechanism

On the basis of all the results reported in this study, a catalytic cycle was proposed for DMC formation over E-SBA-15 catayst, as illustrated in Scheme 5.

In the first and fundamental step of the reaction (1), methanol is activated through a dissociative adsorption to form the alcoholate (CH_3O^-) with the parallel protonation of the amine. In step (2), the methoxy species is able to perform a nucleophilic attack on the EC carbonyl carbon to give a methoxy carbonate anion that, in turn, can be protonated by another methanol molecule (3) to produce the intermediate, 2-hydroxyethyl methyl carbonate (HEMC). A further nucleophilic substitution of HEMC by the CH_3O^- species (4) produces DMC and ethylene glycol anion.

Ultimately, EG can be generated starting from ethylene glycol anion in two distinct steps, that probably occur simultaneously: (5) the proton exchange with a methanol molecule or (6) with a protonated amine of the catalyst. In this way, the catalyst can be regenerated to be employed in a second catalytic cycle.

4. Conclusions

In the present work, the catalytic performances of different amino-modified SBA-15 samples in the carbonate interchange reaction of EC with methanol to produce DMC have been investigated.

The catalytic tests carried out both at 65 and 140 °C suggest that the DMC yield is strictly related to the reaction temperature. Moreover, the high yield of HEMC (the reaction intermediate) obtained at low temperature testifies a close correlation between the stabilization of the reaction intermediate from the different alkylamine chains and the occurrence of the second CIR between HEMC and methanol to produce DMC. Still, no correlation between the catalysts activity and their textural properties (specific surface area and pore size distribution) has been pointed out.

The results of the catalytic experiments were combined with *in situ* FT-IR experimental data and with theoretical calculations

to propose a proper reaction mechanism and to explain the catalytic results observed in the presence of catalysts with different basic strength. In particular, the role played by the different amine chains in activating the reagent molecules and stabilizing the reaction intermediate has been described.

As demonstrated by this multi-technique approach, the ability of the catalyst to dissociatively adsorb methanol is the key factor to select the best catalytic system for this reaction. Moreover, the capacity of the catalyst to stabilize the reaction intermediate (HEMC) has also to be considered in order to allow this species to undergo nucleophilic attack and to form the desired final product (DMC).

In particular, it has been demonstrated that the catalytic activity is inversely proportional to the stabilization capacity of the intermediate and, still, the stabilization of the intermediate on the catalyst surface does not follow the one expected on the basis of the increasing basicity of the alkylamine chains.

All these results highlight that the employment of a multi-technique approach is fundamental for the thorough comprehension of both the reaction mechanism and the catalyst role and, as a consequence, for the rational choice of the best catalytic material and for the optimization of the reaction parameters of the carbonate interchange reaction.

Acknowledgments

This work has been financed with funds of the Italian Ministry MIUR-(project PRIN 2010-2011 n:2010A2FSS9). Thanks are due to Prof. Gabriele Ricchiardi (University of Turin) for the useful discussions.

Appendix A. Supplementary data

Supplementary data associated with this article can be found, in the online version, at http://dx.doi.org/10.1016/j.apcatb.2017.04.013.

References

[1] M. Aresta, A. Dibenedetto, A. Angelini, Chem. Rev. 114 (2014) 1709–1742.
[2] G. Centi, E.A. Quadrelli, S. Perathoner, Energy Environ. Sci. 6 (2013) 1711–1731.
[3] E.A. Quadrelli, G. Centi, J.L. Duplan, S. Perathoner, ChemSusChem 4 (2011) 1194–1215.
[4] P. Tundo, L. Rossi, A. Loris, J. Org. Chem. 70 (2005) 2219–2224.
[5] P. Tundo, M. Selva, Acc. Chem. Res. 35 (2002) 706–716.
[6] Y. Ono, Appl. Catal. A: Gen. 155 (1997) 133–166.
[7] M.A. Pacheco, C.L. Marshall, Energy Fuels 11 (1997) 2–29.
[8] D. Delledonne, F. Rivetti, U. Romano, Appl. Catal. A: Gen. 221 (2001) 241–251.
[9] N. Keller, G. Rebmann, V. Keller, J. Mol. Catal. A: Chem. 317 (2010) 1–18.
[10] T. Sakakura, J.C. Choi, H. Yasuda, Chem. Rev. 107 (2007) 2365–2387.
[11] T. Sakakura, J.-C. Choi, Y. Saito, T. Sako, Polyhedron 19 (2000) 573–576.
[12] M. Wang, H. Wang, N. Zhao, W. Wei, Y. Sun, Catal. Commun. 7 (2006) 6–10.
[13] X.J. Feng, X.B. Lu, R. He, Appl. Catal. A: Gen. 272 (2004) 347–352.
[14] J.O. Jun, J. Lee, K.H. Kang, I.K. Song, J. Nanosci. Nanotechnol. 15 (2015) 8330–8335.
[15] G. Stoica, S. Abello, J. Perez-Ramirez, ChemSusChem 2 (2009) 301–304.
[16] Z.Z. Yang, L.N. He, X.Y. Dou, S. Chanfreau, Tetrahedron Lett. 51 (2010) 2931–2934.
[17] D.J. Darensbourg, C.C. Fang, J.L. Rodgers, Organometallics 23 (2004) 924–927.
[18] D.J. Darensbourg, M.W. Holtcamp, Coord. Chem. Rev. 153 (1996) 155–174.
[19] H.W. Jing, S.K. Edulji, J.M. Gibbs, C.L. Stern, H.Y. Zhou, S.T. Nguyen, Inorg. Chem. 43 (2004) 4315–4327.
[20] H. Kawanami, A. Sasaki, K. Matsui, Y. Ikushima, Chem. Commun. (2003) 896–897.
[21] Y.J. Kim, M. Cheong, Bull. Korean Chem. Soc. 23 (2002) 1027–1028.
[22] X.B. Lu, R. He, C.X. Bai, J. Mol. Catal. A: Chem. 186 (2002) 1–11.
[23] X.B. Lu, B. Liang, Y.J. Zhang, Y.Z. Tian, Y.M. Wang, C.X. Bai, H. Wang, R. Zhang, J. Am. Chem. Soc. 126 (2004) 3732–3733.
[24] X.B. Lu, Y.J. Zhang, K. Jin, L.M. Luo, H. Wang, J. Catal. 227 (2004) 537–541.
[25] R.L. Paddock, S.T. Nguyen, J. Am. Chem. Soc. 123 (2001) 11498–11499.
[26] Y.M. Shen, W.L. Duan, M. Shi, J. Org. Chem. 68 (2003) 1559–1562.
[27] Y.H. Sun, Carbon Dioxide Utilization for Global Sustainability, in: S.E. Park, J.S. Chang, K.W. Lee (Eds.), Elsevier Science Bv, Amsterdam, 2004, pp. 9–16.
[28] B.M. Bhanage, S. Fujita, Y. Ikushima, M. Arai, Appl. Catal. A: Gen. 219 (2001) 259–266.
[29] B.M. Bhanage, S. Fujita, Y. Ikushima, K. Torii, M. Arai, Green Chem. 5 (2003) 71–75.
[30] R. Srivastava, D. Srinivas, P. Ratnasamy, Appl. Catal. A: Gen. 289 (2005) 128–134.
[31] X.H. Zhang, N. Zhao, W. Wei, Y.H. Sun, Catal. Today 115 (2006) 102–106.
[32] B.M. Bhanage, S. Fujita, Y.F. He, Y. Ikushima, M. Shirai, K. Torii, M. Arai, Catal. Lett. 83 (2002) 137–141.
[33] T. Wei, M.H. Wang, W. Wei, Y.H. Sun, B. Zhong, Green Chem. 5 (2003) 343–346.
[34] Z.Z. Yang, X.Y. Dou, F. Wu, L.N. He, Can. J. Chem.: Rev. Can. Chim. 89 (2011) 544–548.
[35] Y. Li, X.Q. Zhao, Y.J. Wang, Appl. Catal. A: Gen. 279 (2005) 205–208.
[36] Y. Kishimoto, I. Ogawa, Ind. Eng. Chem. Res. 43 (2004) 8155–8162.
[37] J.S. Tian, J.Q. Wang, J.Y. Chen, J.G. Fan, F. Cai, L.N. He, Appl. Catal. A: Gen. 301 (2006) 215–221.
[38] J.S. Tian, C.X. Miao, J.Q. Wang, F. Cai, Y. Du, Y. Zhao, L.N. He, Green Chem. 9 (2007) 566–571.
[39] Sujandi, E.A. Prasetyanto, S.E. Park, Appl. Catal. A: Gen. 350 (2008) 244–251.
[40] X.G. Wang, K.S.K. Lin, J.C.C. Chan, S.F. Cheng, J. Phys. Chem. B 109 (2005) 1763–1769.
[41] T. Yokoi, Y. Kubota, T. Tatsumi, Appl. Catal. A: Gen. 421 (2012) 14–37.
[42] S. Saravanamurugan, Sujandi, D.S. Han, J.B. Koo, S.E. Park, Catal. Commun. 9 (2008) 158–163.
[43] S.Y. Chen, C.Y. Huang, T. Yokoi, C.Y. Tang, S.J. Huang, J.J. Lee, J.C.C. Chan, T. Tatsumi, S. Cheng, J. Mater. Chem. 22 (2012) 2233–2243.
[44] D.Y. Zhao, Q.S. Huo, J.L. Feng, B.F. Chmelka, G.D. Stucky, J. Am. Chem. Soc. 120 (1998) 6024–6036.
[45] M.J. Frisch, et al., Gaussian 03, Revision B.05 ed., Gaussian, Inc., Wallingford, CT, 2004.
[46] A.D. Becke, J. Chem. Phys. 98 (1993) 5648–5652.
[47] C. Lee, W. Yang, R.G. Parr, Phys. Rev. B 37 (1988) 785–789.
[48] A. Schäfer, C. Huber, R. Ahlrichs, J. Chem. Phys. 100 (1994) 5829–5835.
[49] C. Møller, M.S. Plesset, Phys. Rev. 46 (1934) 618–622.
[50] S.F. Boys, F. Bernardi, Mol. Phys. 19 (1970) 553–566.
[51] D.Y. Zhao, J.L. Feng, Q.S. Huo, N. Melosh, G.H. Fredrickson, B.F. Chmelka, G.D. Stucky, Science 279 (1998) 548–552.
[52] L.J. Bellamy, Advances in Infrared-Group Frequencies, Methuen, London, 1968.
[53] L. Etgar, G. Schuchardt, D. Costenaro, F. Carniato, C. Bisio, S.M. Zakeeruddin, M.K. Nazeeruddin, L. Marchese, M. Graetzel, J. Mater. Chem. A 1 (2013) 10142–10147.
[54] S. Lowell, J.E. Shields, M.A. Thomas, M. Thommes, Characterization of Porous Solids and Powders: Surface Area, Pore Size and Density, Kluwer Academic Publishers, 2004.
[55] W. Klinthong, K.J. Chao, C.S. Tan, Ind. Eng. Chem. Res. 52 (2013) 9834–9842.
[56] M.H. Lim, A. Stein, Chem. Mater. 11 (1999) 3285–3295.
[57] M. Thommes, K. Kaneko, A.V. Neimark, J.P. Olivier, F. Rodriguez-Reinoso, J. Rouquerol, K.S.W. Sing, Pure Appl. Chem. 87 (2015) 1051–1069.
[58] P. Iliade, I. Miletto, S. Coluccia, G. Berlier, Res. Chem. Intermed. 38 (2012) 785–794.
[59] N.B. Colthup, L.H. Daly, S.E. Wiberley, Introduction to Infrared and Raman Spectroscopy, 2nd ed., Academic Press, New York, 1975.
[60] B. Fortunato, P. Mirone, G. Fini, Spectrochim. Acta 27/A (1970) 1917–1927.
[61] H.Y. Cui, T. Wang, F.J. Wang, C.R. Gu, P.L. Wang, Y.Y. Dai, J. Supercrit. Fluids 30 (2004) 63–69.
[62] A.G. Patil, U.R. Kapadi, D.G. Hundiwale, J. Sci. Ind. Res. 64 (2005) 364–366.